Knitting and weaving artificial muscles

Ali Maziz, Alessandro Concas, Alexandre Khaldi, Jonas Stålhand, Nils-Krister Persson, Edwin W H Jager

APPLIED SCIENCES AND ENGINEERING

Knitting and weaving artificial muscles

Ali Maziz,[1] Alessandro Concas,[1] Alexandre Khaldi,[1] Jonas Stålhand,[2] Nils-Krister Persson,[3] Edwin W. H. Jager[1]*

A need exists for artificial muscles that are silent, soft, and compliant, with performance characteristics similar to those of skeletal muscle, enabling natural interaction of assistive devices with humans. By combining one of humankind's oldest technologies, textile processing, with electroactive polymers, we demonstrate here the feasibility of wearable, soft artificial muscles made by weaving and knitting, with tunable force and strain. These textile actuators were produced from cellulose yarns assembled into fabrics and coated with conducting polymers using a metal-free deposition. To increase the output force, we assembled yarns in parallel by weaving. The force scaled linearly with the number of yarns in the woven fabric. To amplify the strain, we knitted a stretchable fabric, exhibiting a 53-fold increase in strain. In addition, the textile construction added mechanical stability to the actuators. Textile processing permits scalable and rational production of wearable artificial muscles, and enables novel ways to design assistive devices.

INTRODUCTION

The domestication of animals started the quest to augment or replace human power. Water and wind power were followed by steam engines that fueled the industrial revolution, only to be substituted by a wide variety of combustion engines and electrical motors. The latest step in this evolution is the introduction of robotics. Heavy industry, such as car manufactories, already relies heavily on industrial robots; likewise, humanoid robots are now developed to closely interact with humans. Technological revolutions in microelectronics, artificial intelligence, and material science have resulted in a leap forward in robotics, exoskeletons, and prosthetics. Semiautonomous humanoid robots have been created, such as the famous Honda Advanced Step in Innovative Mobility (ASIMO), envisioned to play a major role in taking care of the aging population. Exoskeletons that either enhance human performance or aid disabled people to walk and carry out everyday tasks are becoming commercially available (*1*). Prosthetics, such as artificial hands, have become more intelligent and natural-looking and mimic lost functions rather well (*2*). Recent developments in soft robotics will further enhance assistance robotics (*3*–*5*).

However, these devices are driven by different types of electric motors or pneumatic systems, such as the McKibben Artificial Muscles (*6*). They provide fast responses and have high power densities but are bulky, heavy, stiff, and noisy, being nonbiological in feeling, and as such less accepted by the end user. A paradigm shift is needed where such assistive devices are more biologically realistic, enhancing and attracting usability in everyday life. Ideally, an exoskeleton would be designed as a suit, hidden under clothes, increasing mobility. Thus, there is a great need for novel, lightweight actuators that feel as soft and lifelike, and move as smoothly and silently, as their biological counterpart. A variety of emerging actuator technologies have been reported, including dielectric elastomers (*7*), piezopolymers (*8*), carbon nanotubes (*9*), shape-memory polymers (*10*), phase transition actuation (*11*), and thermal actuation (*12*). Although they have issues such as high driving potentials, low strain, or thermal kinetics, they also show that structuring these materials is important for their performance. For instance, carbon nanotube yarns (*13*, *14*), nylon actuators (*12*), and shape-memory alloy (SMA) wires (*15*, *16*) have been structured into patterns that can accomplish high actuation forces or rotational actuation.

Here, we present the concept of textile actuators. By combining one of humankind's oldest technologies—textile processing, here in the form of weaving and knitting—with new advanced materials, such as electroactive polymers, we fabricate a new kind of textile actuators ("textuators"). These textuators scale up force by parallel assembly of single fibers (Fig. 1A), amplify the strain by using stretchable patterns (Fig. 1B), and can be effectively mass fabricated. This will allow for a new means of driving and designing assistive devices, such as exoskeleton-like suits with integrated wearable actuators.

Textile processes are an excellent means to efficiently assemble fibers, and hundreds of years of industrial development have perfected the processes. Efficient production enables high-quality and extremely cost-effective products with a high degree of repeatability. The fibers used in textiles are of different classes: monofilaments, one single continuous strand; multifilaments, consisting of more than one continuous strand; and staple yarns, consisting of small (centimeter to decimeter) fiber segments (staples) twisted together. Unfortunately, the nomenclature is not always consistent, and we will use yarn as the umbrella term. Weaving and knitting are the two foremost textile processing methods. Weaving has two perpendicular and individual tread systems, warp and weft threads, that come close contact and result in a rigid fabric. In knitting, the yarns are kept together by loops that give a latent potential for being easily deformable. The many inherent advantages of textiles—wearability, pliability, high surface area, and omnipresence—led to the development of smart textiles, where textiles and other technologies, not least electronics, merge. Smart textile supercapacitors, high–surface area electrodes, and strain sensors have recently been developed (*17*–*20*).

RESULTS AND DISCUSSION

To demonstrate the feasibility of textile actuators, we used here the conducting polymer (CP) polypyrrole (PPy) as the active material that deforms in response to electrical stimulation, because the physical and chemical properties of PPy have been well characterized (*21*–*23*). In short, PPy undergoes a volume change upon electrochemical oxidation or reduction by applying a low potential of

[1]Department of Physics, Chemistry and Biology (IFM), Biosensors and Bioelectronics Centre, Linköping University, 58183 Linköping, Sweden. [2]Department of Management and Engineering (IEI), Solid Mechanics, Linköping University, 58183 Linköping, Sweden. [3]Swedish School of Textiles (THS), Smart Textiles, University of Borås, 50190 Borås, Sweden.
*Corresponding author. Email: edwin.jager@liu.se

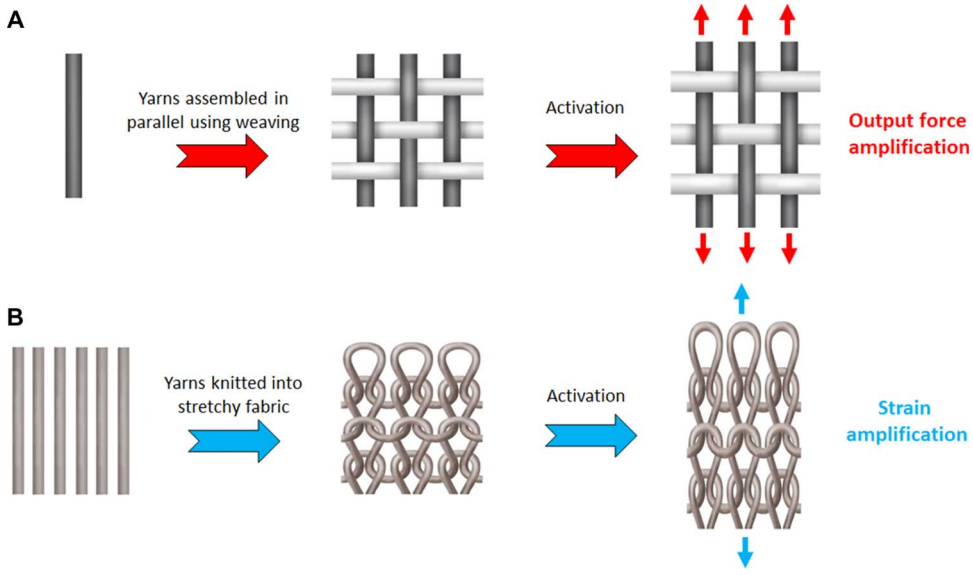

Fig. 1. Concept of the textile actuators (textuators). (**A**) The textuators scale up force by weaving of single yarns in parallel. (**B**) The textuators amplify the strain by using stretchable knitted patterns.

1 to 2 V. The reversible volume change is predominantly caused by the insertion or ejection of ions and solvents into the polymer matrix. This volume change is used to build actuators in different configurations and sizes, from a self-propelled robotic fish (*24*) down to microscopic robots (*25*, *26*). Because the volume change is based on ion and solvent motion, the CP actuators need an ion source/sink to operate. This may be an electrolytic solution or a solid polymer electrolyte, which allows operation in normal atmospheric conditions. PPy actuators deliver high stresses, typically a few megapascals, exceeding mammalian skeletal muscles that deliver stresses of 0.35 MPa (*27*), are silent, and are driven at low voltages. There is a huge interest in replacing oil-based fibers with renewable cellulosic fibers. Therefore, we used cellulose-based yarns as the core material, thus opening up a new range of functionalization for this material class. Previous studies (*28*, *29*) showed that hydroxyl groups are good anchoring points for the CP poly(3,4-ethylenedioxythiophene) (PEDOT). Cellulose materials are biocompatible, compostable, and produced by a renewable, green chemistry (*30*). We used single (S) (~200 μm in diameter) and two-ply twisted (T) cellulose-based (Lyocell) staple yarns. We assembled the yarns into two different textile constructions, a twill 4/4 weave and a 2:1 rib knitwear, using standard industrial textile production machines, a 150-cm-width weaving machine (Dornier GmbH) and a flat knitting machine (Stoll AG & Co.), respectively. Figure 2A shows the highly stretchable knitted fabric made.

We have chosen to first fabricate the fabrics and thereafter coat them with the electroactive polymers, similar to the dyeing process routinely used in textile fabrication, using a two-step chemical-electrochemical synthesis resulting in metal-free textile actuators (fig. S1), providing an effective fabrication of large conductive textiles. More specifically, first, a chemically synthesized PEDOT "seed layer" is deposited to form a highly electrically conductive surface, allowing the consecutive electrochemical deposition of the functional, actuating PPy layer. To achieve a uniform coating of the PEDOT seed layer, we used vapor-phase polymerization (VPP) of 3,4-ethylenedioxythiophene (EDOT) doped with p-toluenesulfonate (PEDOT:Tos) from an iron(III) p-toluenesulfonate [$Fe(Tos)_3$] in butanol solution (*31*) with a fraction of polyethylene glycol derivatives. Previous work showed that the addition of a glycol-based surfactant to the $Fe(Tos)_3$ solution has a positive effect on the synthesis of highly conducting PEDOT (*32*). The additives act as surfactants, resulting in a homogeneous distribution throughout the material and a decrease of the electrical resistance along the conductive textile (table S1). Next, PPy was galvanostatically electrosynthesized from a pyrrole and lithium bis(trifluoromethane)sulfonimide (LiTFSI) propylene carbonate solution, as described in Materials and Methods and shown in fig. S2. Scanning electron microscopy (SEM) showed a uniform coating of the PEDOT-PPy layers and that the initial fibrous structures of both single (S-yarn) and twisted (T-yarn) yarns are retained well after the PEDOT-PPy coatings (Fig. 2, A and C). Not only individual yarns but also complete fabrics can be uniformly coated using this method. Figure 2 (D and E) shows a large area weave (10 cm by 10 cm, limited only by the size of our deposition equipment) coated with PEDOT and PEDOT-PPy, respectively. Figure 2 (F and G) shows the homogeneous distribution of the CPs on the woven and knitted fabrics, confirmed by energy-dispersive x-ray spectroscopy (EDX) with a sulfur mapping over the fabrics' surfaces, because sulfur atoms can be considered the chemical signature of PEDOT (via sulfur atoms) and PPy (via dopant). The conductive textile surface coverage was found to be an important parameter for the textile actuator. The textile coverage of CPs was controlled by varying the weight content of the PEDOT [2.0 weight % (wt %)] and PPy (20.0 wt %) in the two-step chemical-electrochemical synthesis (for more details, see the Supplementary Materials). To investigate the penetration of the PEDOT/PPy into the Lyocell yarn, we took SEM-EDX measurements of the cross section of the yarn (fig. S3). The PEDOT/PPy coating appears to be concentrated near the surface and slightly penetrating into the Lyocell yarn, suggesting a seamless connection between the PEDOT/PPy and the Lyocell core, thereby providing the good adhesion essential for good operation. An effective thickness of 14 ± 3 μm of the chemically-electrochemically synthesized CP coating was estimated from the EDX images.

Electromechanical testing was performed by immersing the coated textiles (that is, individual S-yarn or T-yarns, and knitted or woven

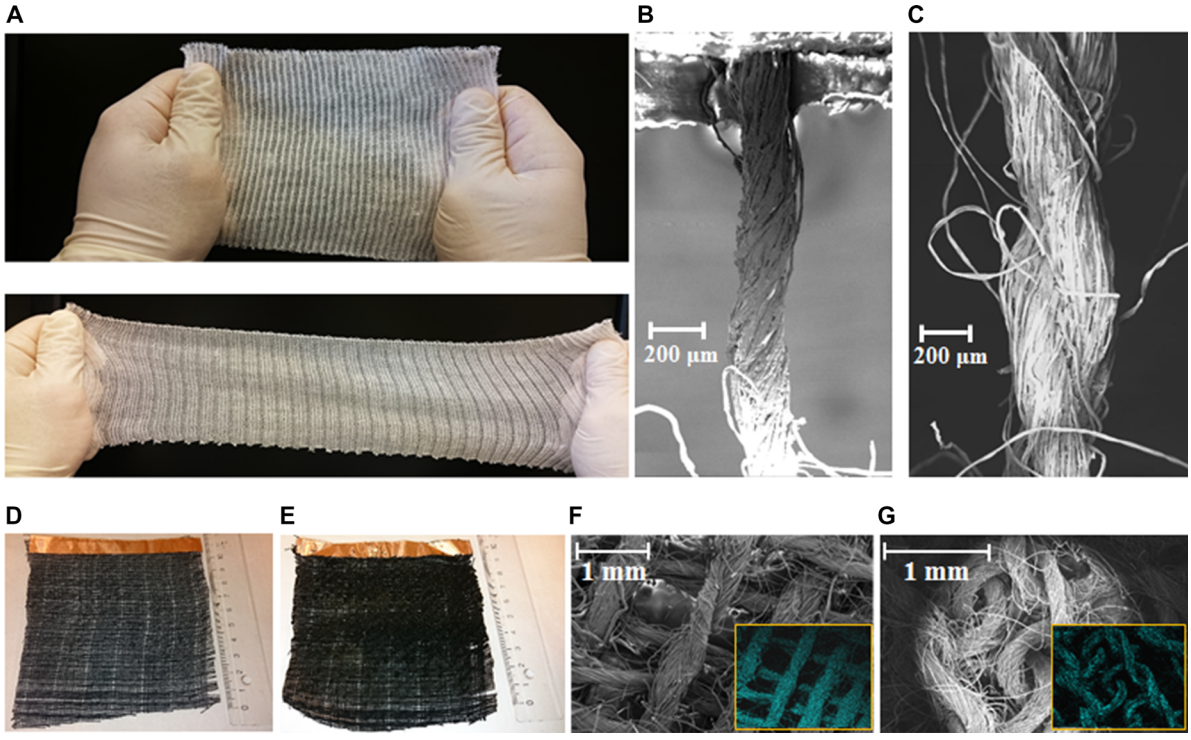

Fig. 2. Textile actuators manufacturing. (**A**) Photograph of a Lyocell-based knitwear between 0% strain (unstretched state) and 220% strain (stretched state). (**B**) CP coated Lyocell-based single yarn. (**C**) CP-coated Lyocell-based twisted yarn. (**D**) Photograph of VPP PEDOT–coated (2.0 wt %) Lyocell-based weave. (**E**) Photograph of PEDOT-PPy–coated Lyocell-based weave. (**F**) SEM image of PEDOT-PPy–coated Lyocell-based weave with 2.0 wt % PEDOT and 20.0 wt % PPy. Insert: An EDX sulfur map over the conductive weave textile. (**G**) SEM image of PEDOT-PPy–coated Lyocell-based knitted fabric with 2.0 wt % PEDOT and 20.0 wt % PPy. Insert: An EDX sulfur map over the conductive knitwear.

fabrics) in a three-electrode system consisting of a LiTFSI propylene carbonate solution, a reference electrode, and a gold-coated polyethylene terephthalate counter electrode. An alternating potential of −1.0 and 0.5 V was used to reduce and oxidize the PEDOT-PPy. First, a few equilibration cycles were applied for each new sample used, because previous observations showed that the material changes its properties after the first electrochemical stimulation (*33*, *34*).

To confirm the ion motion, we measured the charge-induced radial swelling of an individual S-yarn (fig. S4). The yarn actuator expanded during the cathodic wave, confirming that cation motion (including solvent) is the main driving mechanism in these actuators (*35*, *36*). The diameter change of the PPy-coated yarn is 2 µm, which corresponds to a 14% radial thickness change of the 14-µm-thick PPy coating, in agreement with previous results that show a large perpendicular volume change of PPy(DBS) specifically (*33*, *37*).

Using the Lever Arm Dual Mode Servo System (fig. S5), we measured isometric force and isotonic strain. When the sample is immersed in the electrolyte, it undergoes some solvent swelling; thus, to remove this initial slack, the sample was prestretched by applying a load of 1 g. Next, we applied a square wave potential (+0.5 and −1.0 V), and the yarns contracted and expanded upon oxidation and reduction, respectively. Figure 3 (A and B) shows the linear actuation response of an individual T-yarn. The individual yarn exerted an isometric force of 8.0 ± 0.5 mN and an isotonic strain of 0.140 ± 0.005% relative to the equilibrium strain caused by the applied load. The resulting strain is lower than typically observed for pure PPy films (*38*–*41*) but similar to other CP devices (*42*). The stress, calculated from the 20% PPy ratio, is 0.50 ± 0.05 MPa, similar to that obtained previously (*43*).

The relatively low strain value can be explained by the mechanical properties of the Lyocell yarn that forms the passive core of the actuating yarn. Tensile stress measurements of the Lyocell yarn are shown in fig. S6. The individual Lyocell yarn has a Young's modulus, obtained from the initial slope, of 26 MPa, making the Lyocell yarn (that is, the core) relatively stiff, resulting in the relatively low strain of the PPy-coated yarn. The strain of the individual yarn can be altered by changing the yarn (core) material. For instance, by using an elastane yarn that has a lower Young's modulus (E = 0.015 MPa) as the core, we increased the single yarn strain from 0.075% for the PPy/Lyocell yarn to 0.3% for the PPy/elastane yarn (fig. S7). Likewise, using thin, stiff metal yarns (thin monofilament wires, E = 1.1 GPa) as the core resulted, as expected, in no measurable elongation of the yarn (fig. S6). In addition, the strain can be increased by optimizing the synthesis parameters of the PPy coating (*40*, *44*–*46*).

As mentioned, CP actuators generate high stress; however, the exerted forces are typically low. As has been described in several reports (*21*–*23*, *46*–*48*), the actuation mechanism in CPs is dominated by mass transfer, including ions and solvents into the polymer. Therefore, the actuation speed will be determined by diffusion rate and diffusion distance (*48*). Thus, to keep a moderate actuation speed, only thin layers or fibers of CPs are used; hence, the exerted forces are typically low. Previous work demonstrated higher actuation forces by increasing the thickness and/or the cross-sectional area by complex and time-consuming assembling of macrodevices, operating at very low strain and low speed (*41*, *49*). A first characteristic of textile technology is that it allows rational parallel assembly of fibers/yarns, and this increases the total force of the actuators while

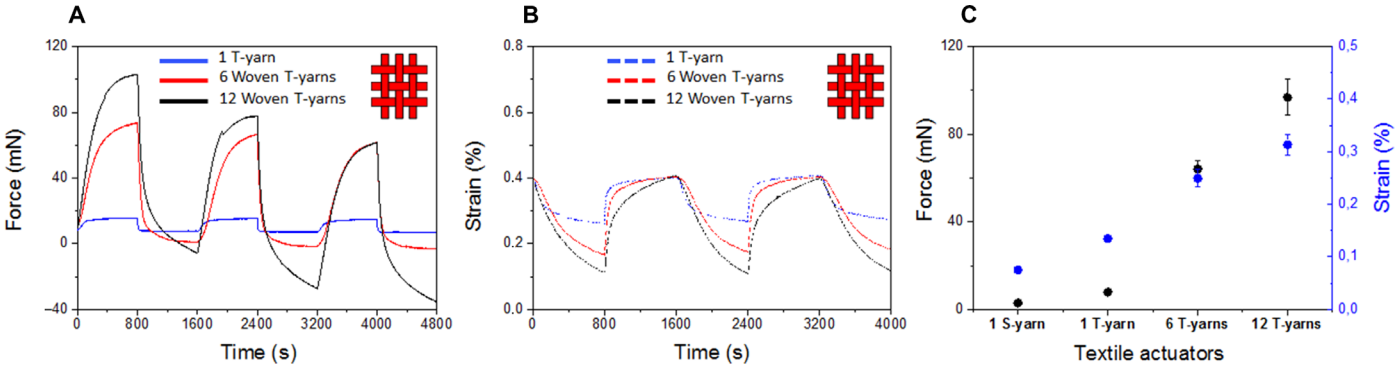

Fig. 3. Electromechanical characterizations of the woven textile actuators. (**A**) Measured isometric force and (**B**) isotonic strain ($\Delta L/L_0$) versus time for individual T-yarn, 6 T-yarn weave, and 12 T-yarn weave during activation between 0.5 and −1 V for 800 s. (**C**) A comparison between the measured isometric force and the isotonic strain of the individual yarns, 6 T-yarn weave, and 12 T-yarn weave as average of five measurements.

conserving the strain and keeping the advantages of single, thin yarns, that is, a high surface-to-volume ratio. To illustrate this effect, we have taken the simplest assembly, here a simple plain weave of T-yarns (Fig. 2F). We compared the performance of a single yarn and weaves of various widths, that is, having different numbers of vertical yarns (Fig. 3A and B). The absolute output force increased and was proportional to the number of parallel-assembled CP yarns in the weave. For instance, a textuator weave with 6 parallel yarns exhibited a force of 64 ± 4 mN, and with 12 parallel yarns exhibited a force of 99 ± 8 mN, compared to the individual T-yarn (8.0 ± 0.5 mN) (Fig. 3C). Surprisingly, we also observed an increase of the strain of the 6- and 12-yarn weaves compared to the individual T-yarn, which we attribute to the fact that the vertical warp yarns in the weave are not perfectly straight but slightly undulating from passing under and over the horizontal weft yarns in the textile architecture. The isometric force of an individual S-yarn is half the force of an individual T-yarn. The particular T-yarn used could be considered as two S-yarns twisted together, thus having twice the PPy cross-sectional area and twice the force. The increased strain of the single T-yarn compared to the S-yarn can also be explained by this twisting. During activation, the T-yarns twist and untwist, which amplifies the motion, as seen in the twisted fishing line actuators (*12*).

Although the textile actuators were studied under the same conditions, the actuation performance for the individual yarns quickly reached a pseudoplateau, whereas in the woven textiles, both force and strain still slowly increased at the end of the cycle. To evaluate the actuation profile of the textile actuators within a redox cycle, we assessed the speed of the actuators during contraction (oxidation) and elongation (reduction), respectively. To permit a fair comparison between the different reported data, we adopted an actuation metric that was recently reported by Melling *et al.* (*33*). The metric consists in the time taken for the actuator to expand or contract to 90% of its maximum value during the scan. This metric takes into account the differences imposed by the used fiber core material and/or textile pattern. Figure 4 (A and B) summarizes the time values to 90% of maximum contraction and elongation as a function of the textile actuator used. It was observed that for all samples, the times are longer during the oxidation scan (contraction) than the reduction scan (elongation), confirming previously reported data (*33*, *37*, *50*). For instance, the contraction time was ~390 s for the single T-yarn, ~600 s for the 6 parallel T-yarns, and ~620 s for the 12 parallel T-yarns, although the elongation times decreased to ~250 s for the single T-yarn, ~290 s for the 6 parallel T-yarns, and ~510 s for the 12 parallel T-yarns. These results show that the actuation speed is faster during the reduction scan compared to the oxidation scan, which is attributed to the higher electronic conductivity of CPs in the oxidized state. Upon reduction, the CP starts in the conducting state and is converted into the insulating state, and vice versa upon oxidation, causing the so-called iR (voltage) drop to be different, which effectively leads to nonsymmetric oxidation and reduction processes (*33*, *37*, *50*). It was also found that the elongation and contraction times for the actuators increase with the number of parallel-assembled CP yarns in the weave (Fig. 4, A and B). This result can be explained by the diffusion phenomena of ions and solvent into CP that drives the volume change. For the single yarns, a radial diffusion profile for the charge-compensating ions during the redox switching is expected, whereas the fabrics have a more planar diffusion profile and increased electroactive surface area. Further improvement in performance is expected with our next generation of textile actuators produced with thinner yarns, which will enable faster ion diffusion rates. The clear effect of the yarn diameter on ion diffusion is seen in Fig. 4 (A and B). The elongation and contraction times of the S-yarn (~200 μm in diameter) are shorter than those of the T-yarn (~400 μm in diameter). In addition, optimizing the CP textile actuators with respect to electrolyte concentration (*46*) or applied stimulation profile (*27*) will further improve actuation performance for the CP textile actuators.

Figure 3 (A and B) also indicates that a certain amount of creep is associated with the response of the textile actuators. It is widely accepted that almost all textile materials and CP actuators exhibit an appreciable amount of extension with time under the influence of mechanical stresses (*51*). The core material and structure of the textiles, as well as the volume ratio of the CPs, affect the creep behavior of textile actuators (*52*, *53*).

Another advantage is that the textile actuators can sustain higher loads before failure than a single fiber or yarn. Moreover, the yarn-interlacing construction of the textile assembly gives the actuator a dimensionally stable structure with reduced tendency to fatigue and more stable operation. We evaluated the stability of the woven textuator by cycling the 12 T-yarn weave between −1 and 0.5 V at 0.05 Hz (Fig. 5). The textuator showed a stable actuation force for the first 1500 cycles, which thereafter gradually decreased by ~27% until 2500 cycles and remained stable for the remaining period until

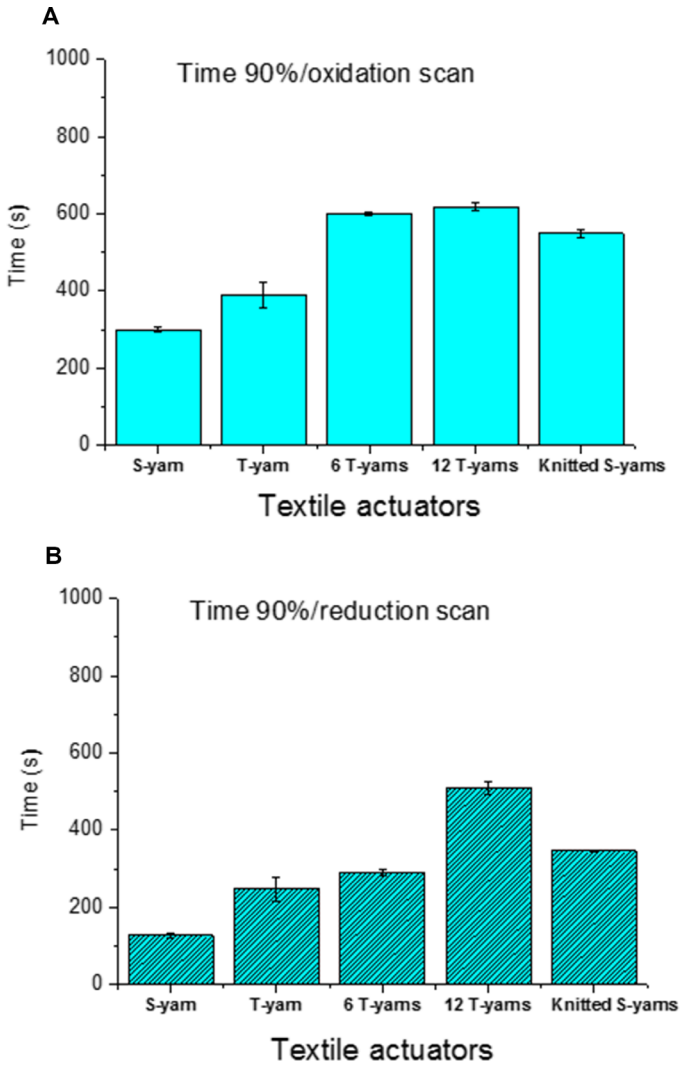

Fig. 4. Evaluation of the actuation speed for the textile actuators. Time to 90% maximum contraction (oxidation scan) and elongation (reduction scan) for individual S-yarn, individual T-yarn, 6 T-yarn weave, 12 T-yarn weave, and knitted S-yarns during activation between 0.5 and −1 V for 800 s.

the test stopped at 8000 cycles (~45 hours). This indicates that the textile construction adds mechanical stability, reducing the decrease in performance that has been observed in PPy linear actuators (*52*, *54*). The reduction in performance might be caused by parasitic reactions leading to structural changes along the PPy backbone and hence to a lower capacity to generate movement after several hundreds of cycles (*55*). It has been shown that, at higher current densities, parasitic reactions start to occur (*54*). We did measure an increase of the (oxidation) peak current from 7 mA in the first hundred cycles to ~14 mA for the last hundred cycles (fig. S8), which may confirm this. We believe that further improvements in stability of the textile actuator can be achieved by optimizing the stimulation profile.

A second characteristic of textile technology is that it allows the production of advanced architectures, such as highly stretchable fabrics. We used this property to amplify the strain of the actuators. Figure 2A shows a 2:1 rib knitwear from Lyocell S-yarn. The knitwear was functionalized with the same PEDOT-PPy coating as the weave. Figures 6A and 4B show the isometric force and isotonic strain, respectively, of a single S-yarn and a 10-mm-wide knitted fabric. As for the woven fabric, the elongation and contraction times for the knitted fabric are higher than those of the individual S-yarn (Fig. 4, A and B). The isotonic strain increased from 0.075% for the single yarn to 3% for the knitted fabric, that is, a 53-fold amplification of the strain due to the textile architecture. Unlike the plain weave where two sets of yarns are interlaced at right angles (fig. S9), knitted constructions are made up of rows and columns of loops interlinked with each other. The row is known as a course, and the column is a wale (Fig. 7A) (*56*). The knitted construction is more open, leading to a greater degree of yarn mobility (*57*), and provides the actuator a greater compliance and strain amplification. We propose a semiquantitative explanation for the strain amplification in textile actuators, as illustrated in Fig. 7B. We take the well-known dry-to-wet swelling behavior of fabrics (*58*) as a starting point for this model because it is analogous to the electrochemically induced volume change caused by the insertion and ejection of ions and solvent (*21*, *22*). The typical actuation cycle is initiated from a prestressed state where the initial slack between the interloping yarns has been removed by applying a small tensile load of 1 g to the fabric [Fig. 7B(i)]. A negative potential of −1.0 V is applied to electrochemically reduce the PPy. Cations and solvent molecules are subsequently inserted into the PPy to ensure the overall electroneutrality, resulting in a volume change of the PPy and an elongation of the yarn. The yarn elongation causes the loop to elongate, increasing the course height while slightly reducing the wale width [see Fig. 7B(ii)]. Because the loops are interconnected and seamlessly associated to the adjacent courses of loops, the macroscopic fabric strain is the integrated effect of all individual loop changes in height, width, and curvature. As a result, the textile actuator presents a net macroscopic strain, which is considerably higher than the local strain within the yarn itself, thus amplifying the strain. This result agrees with previous reports describing strain in glass fiber composite fabrics (*57*) and thermally actuated SMA knit patterns (*15*), and is also conceptually analogous to the undulator and C-block models of Benslimane *et al.* (*59*). When a positive potential of 0.5 V is applied to oxidize the PPy, the process reverses: cations and solvent molecules are expelled from the polymer, and the yarn contracts, closing the loops and reducing the course height, thus inducing a contraction of the entire textile [Fig. 7B(iii)]. A complementary macroscopic model, to explain the

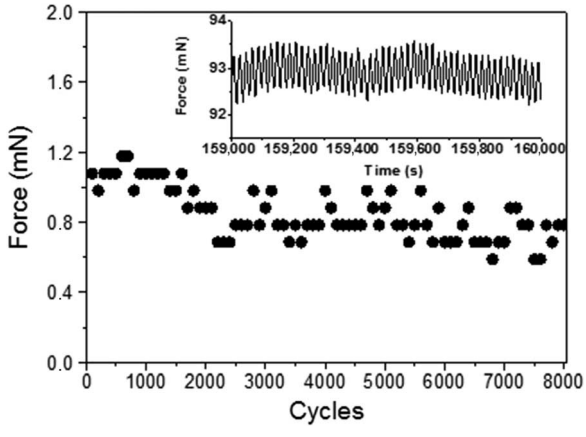

Fig. 5. Life cycle test of the woven textile actuators. Life cycle test of 12 T-yarn weave during activation between 0.5 and −1 V for 10 s for 44 hours. Insert: Measured force versus time of the last 50 cycles of the life cycle test.

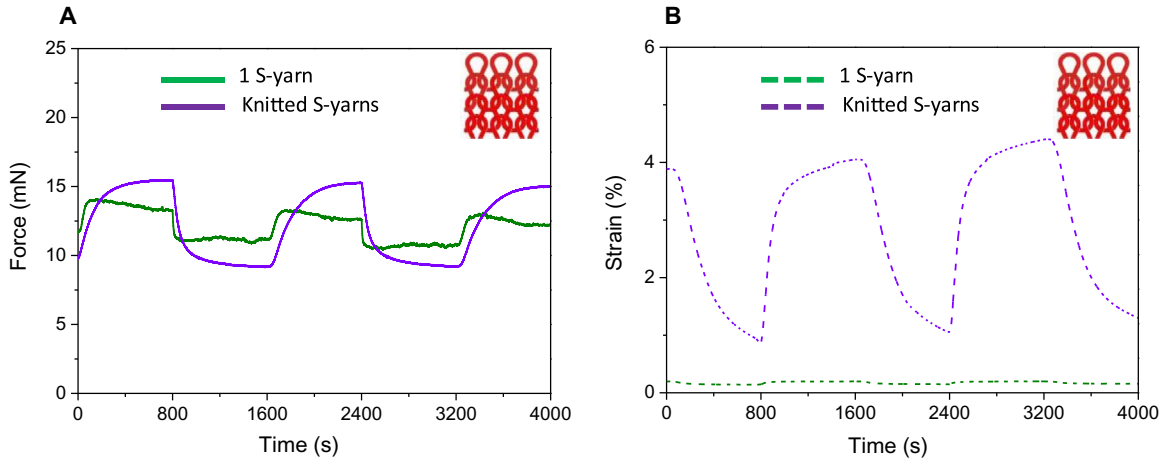

Fig. 6. Electromechanical characterizations of the knitted textile actuators. Measured (**A**) isometric force and (**B**) isotonic strain ($\Delta L/L_0$) versus time for S-yarn and knitted S-yarn fabric during activation between 0.5 and −1 V for 800 s.

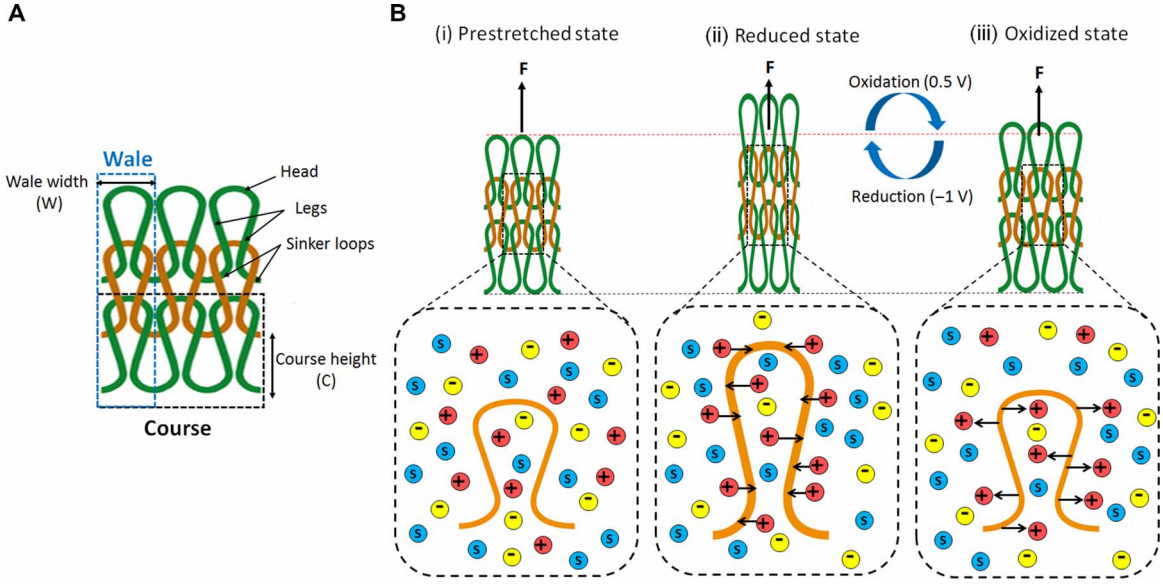

Fig. 7. Semiquantitative model of the knitted textile actuators. (**A**) Definition of knitting terms. (**B**) Schematic description of the actuation process. The fabric is inserted in an electrolyte solution containing cations (+), anions (–), and solvent molecules (S). The actuation starts by prestretching the fabric to remove the initial slack between the interlooping yarns (i). When reducing the PPy, cations are inserted into the yarn, causing an elongation of the yarn and a loop elongation (ii). Subsequent oxidation of the PPy causes the ions to be expelled, the yarn shrinks, and the loop closes, resulting in a net contraction of the fabric (iii).

strain amplification, is based on the macroscopic stress-strain response of a single yarn, a weave, and a knitwear, as illustrated in Fig. 8. The single yarn has the stiffest initial response (highest Young's modulus) followed by, in turn, the weave and the knitwear. The decreasing stiffness in the fabrics is linked to the yarn undulation (weave) or looping (knitwear). The yarns in the fabrics reorganize, for example, the loop elongation closing in knitwear as explained above, at low strains causing a low fabric stiffness; if the strain increases further, then the yarns gradually straighten and finally form what can be considered parallel single yarns, increasing the fabric stiffness. In this high strain limit, an ideal fabric, without yarn entanglements and yarn-to-yarn friction, attains the Young's modulus of the single yarn. Therefore, the textile construction causes a bilinear-like or exponential stress-strain response for the weave and knitwear (Fig. 8). When the PPy is reduced and swells, the stress in the single yarn, or the fabric, increases. This causes a lengthening to a new higher equilibrium strain [Fig. 7B(ii)]. Because of these differences in the stiffness, the lengthening will be larger in the knitwear and the weave compared to the single yarn, thus explaining the strain amplification. It should be noted that knitted construction exhibited a lower force than woven construction (Figs. 3C and 6A). The isometric force for the knitted textile actuator shows a moderate ~2-fold increase compared to the individual S-yarn (2.9 ± 0.1 mN). Reduced force output is a typical trade-off in strain amplification strategies (*60*). We are currently investigating in more detail the effect of textile architecture on performance.

As mentioned, the strain can be further tuned by the yarn core material and knitted architecture, indicating the universality of the textuator concept. For instance, by using a soft elastane yarn as the core, the single yarn strain was increased from 0.075% for the Lyocell to 0.3% for elastane. By knitting these elastane yarns in a 1:1 rib pattern

(compared to 2:1 rib fabric of Lyocell), the strain was amplified 10-fold (0.3 to 3%) (fig. S7). Likewise, using stiff metal yarns as the core resulted in no measurable elongation of the yarn, but, when assembled into a 3-cm-long stretchy metal fabric, we measured a 96-μm elongation (fig. S10).

Figure 9 shows the frequency responses for both individual yarns as well as the knitted and woven fabrics. The maximum electromechanical responses were obtained at the lowest measured frequency, 6.25 10^{-4} Hz, and decreased as the frequency of the input potential increased. Because the actuation principle in CPs is mainly ruled by the ion transfer (including solvent) through redox reactions, the actuation speed is mainly determined by diffusion rates (*21*, *47*, *48*). By optimizing the surface-to-volume ratio of the PPy in the yarn or using thin all-PPy yarns to decrease the ion diffusion times, the performance, especially speed, can be further improved. For instance, using thin PEDOT layers, 1.4-kHz operation of a CP trilayer actuator has been achieved (*61*). We are currently optimizing the ratio and investigating thin all-PPy yarns. Other parameters that can be further optimized to increase the speed are electrolyte concentration (*46*, *47*) and applied stimulation profile (*27*).

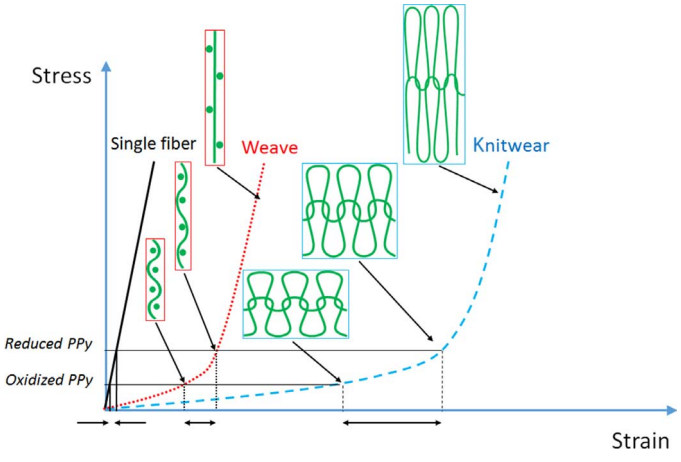

Fig. 8. Macroscopic stress-strain responses of the textile actuators. The single yarn has the stiffest initial response (highest Young's modulus) followed by, in turn, the weave and the knitwear. The textile construction, that is, yarn undulation (weave) or looping (knitwear), results in decreasing stiffness in the fabrics and causes a bilinear-like or exponential stress-strain response. When the PPy is reduced and swells, the stress in the single yarn, or the fabric, increases and causes a lengthening to a new higher equilibrium strain. Because of differences in the stiffness, the lengthening will be larger in the knitwear and the weave compared to the single yarn resulting in strain amplification.

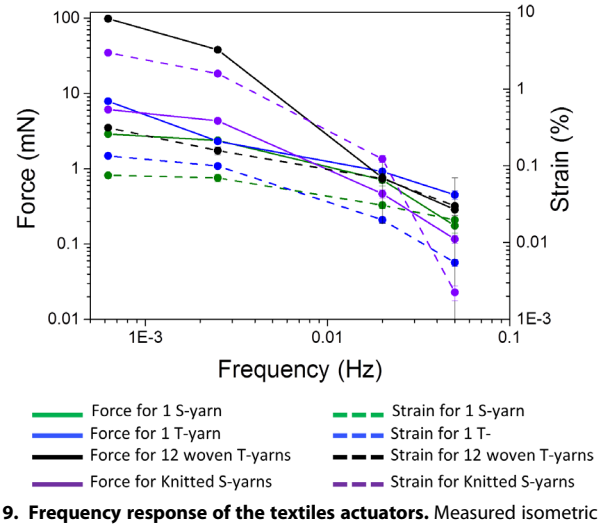

Fig. 9. Frequency response of the textiles actuators. Measured isometric force and isotonic strain ($\Delta L/L_0$) versus frequency for individual S-yarn, individual T-yarn, 12 T-yarn weave, and knitted S-yarn during activation of the actuators between 0.5 and −1 V for 800, 200, 25, and 10 s, average of five measurements.

To demonstrate the feasibility of integrating textile actuators into soft robotics, we designed a textuator unit of a knitted fabric (Fig. 10A) and integrated this in a LEGO lever arm. The textuator unit was mounted in an electrochemical cell, comprising counter electrode, reference eletrode, and the electrolyte that was integrated into the lever arm. Only about half of the textuator unit was submerged in the electrolyte, meaning that only ~3 cm was active. The textuator could smoothly move the arm, lifting a 2.0-g weight attached at distal end (Fig. 10, B to D, and movie S1). Considering the lever arm ratio and weight, this means that the exerted force of the textuator was 125 mN and the work 59 mJ (excluding the friction at the pivot point).

CONCLUSIONS

Here, we demonstrated the feasibility of textile actuators and the advantages of using advanced textile technology, such as increased force by parallel assembly, increased strain by using a knitting pattern, and added mechanical stability. The introduction of textile processing to the actuator field enables both upscaling in terms of force and strain of a single actuator and upscaling in terms of efficient production.

Textile technology is open to a wide range of improvements and modifications. Here, we used only a limited number of textile constructions. Textile patterning, originally developed for aesthetical reasons, also offers great opportunities to embed functionalities. A plethora of materials can be woven and knitted, including metals, carbon fibers, and polymers, as well as more traditional textile materials such as cotton and synthetic yarns. The various materials can be mixed into the fabrics during the weaving or knitting process. Metal wires may be added to increase the conductivity (Fig. 11A). Stiffer materials may be used in the horizontal wefts to increase the anisotropic movement. We envision adding sensing yarns into the fabric to allow sensing displacement and thus allow better control through a feedback system, thus developing multifunctional textiles. By cleverly exploiting the various weaving and knitting architectures, we can optimize the performance of the textuator toward a specific application. That is, we can design the fabric to give a large force, for example, by using a plain weave, or a very large strain, by using an extremely stretchable knitting pattern, or anything in between. Furthermore, totally novel textile constructions can be developed, which are relevant for actuating functionality. Figure 11B shows an example of a weave with spacing custom-designed to enable movements of yarns. We will explore these bespoke constructions further. The CP-based knitted textile is a promising smart architecture for an actuator application. However, the textile actuator is a highly complex three-dimensional structure where electrochemical, mechanical, and tribological (friction between yarns) phenomena interact. To harvest the potential of this new concept, a detailed model for textile actuators needs to be further developed.

Here, we showed that the fabrics can be functionalized using a coating process similar to dyeing of textiles. Likewise, electroactive yarns can be directly assembled into the fabric. We coated yarns with

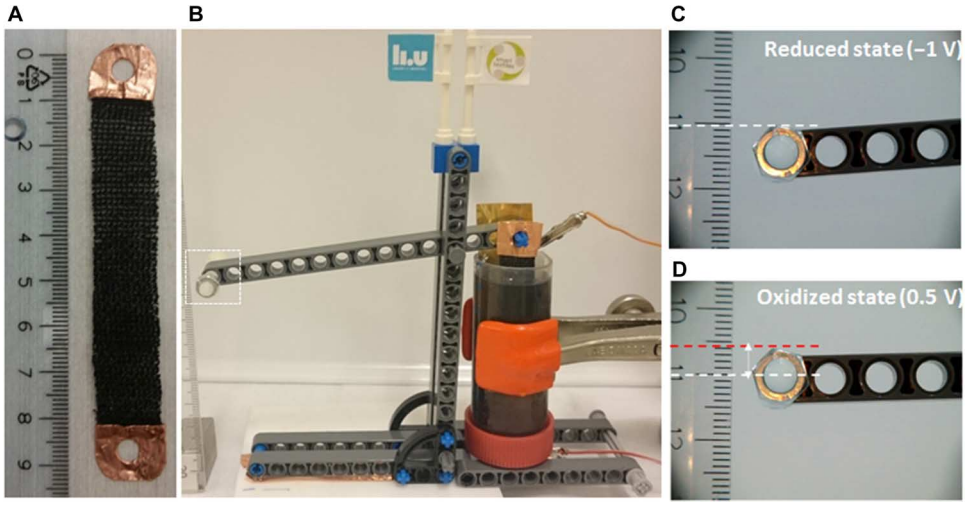

Fig. 10. Applications of the textile actuators. (**A**) A knitted textuator unit. (**B**) The textuator unit (~3-cm active length) drives a lever arm in a LEGO setup. The arm lifted a 2.0-g load when switched between −1 (reduced state, **C**) and 0.5 V (oxidized sate, **D**).

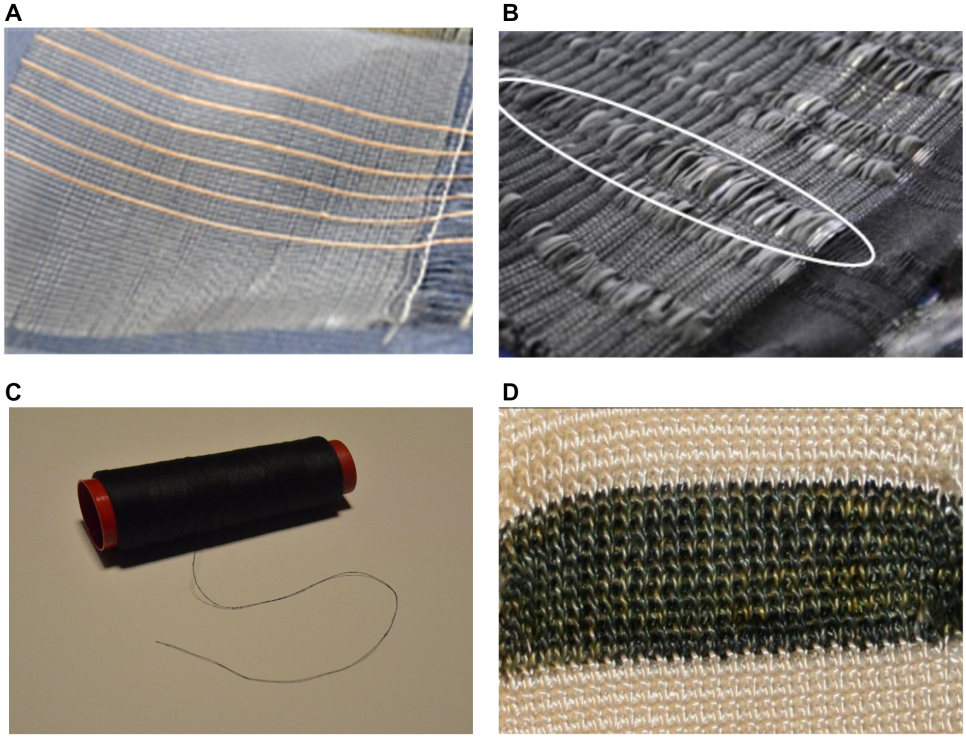

Fig. 11. Processing and integration of electroactive textiles. (**A**) Cu monofilaments in weave fabric. (**B**) Example of a custom weave with spacing (marked) that enables movements of yarns within the marked area. (**C**) A bobbin with industrially manufactured PEDOT-coated yarn. (**D**) A knitwear structure for respiratory monitoring comprising CP-coated yarns (black yarn) knitted together with normal (white) yarn.

PEDOT in an industrial process (Fig. 11C) and assembled those conducting yarns into an electroactive fabric (Fig. 11D). We have already demonstrated that these wearable smart textiles can be used in sensing applications (*62*). PPy fibers have also been made using wet spinning (*63*).

Actuation based on CP was chosen to demonstrate the concept among other reasons because CPs can be easily coated on standard yarns, but operating CPs requires an electrolyte, here in the form of LiTFSI in propylene carbonate. Using ionic liquids enables operation of CP actuators in air (*64*) or space conditions (*65*) and, they may be used for CP-based textile actuators. The concept of textile actuators can be applied to other, "dry" actuation means as well, such as piezoelectric polymers or thermal expansion. We are currently working on the second generation of wearable textile actuators that operate in air.

We showed that the CP-based textuators can be integrated in a simple robotic device, such as a LEGO lever arm (Fig. 10B); however,

textile actuators allow for innovative designs. We envision integration of textile actuators, based on any actuation means, into clothing, such as tights, forming an exoskeleton suit that can be worn to assist walking, or socks and sleeves, applying compression to relieve edema. Although there still is a long way to go to generate a true artificial muscle, the textile actuator concept introduced here presents a small step forward. We envision a future where we will be able to shake the hand of an amputee knowing that intelligent prosthetics driven by soft, compliable textile actuators made the gesture possible.

MATERIALS AND METHODS

Textile manufacturing

Single (S) and two-ply twisted (T) Lyocell cellulose staple yarns were used. For weaving, a twill 4/4 (every weft thread goes above four warp threads and under four) construction was used with a warp density of 11.25 tr/cm to achieve a loose, flexible material fabricated on a positive rapier, 150-cm-width weaving machine (Dornier GmbH) with 16 shafts used, having normal, industrial single-phase beating-up operation. The knitted fabric was 2:1 rib knitwear made on a CMC 330 flat knitting machine (Stoll AG & Co.) with gauge 10 and 2 yarn carriers. Warp: CO Nm 50/2 yarn with 22.5 tr/cm in total and 11.25 tr/cm. Weft: LY (Lyocell), Tencel (Lenzing AG) Nm 30/2. Also, 1:1 rib knitwear was produced on the same machine, containing elastane (PA/Lycra dtex 78–44 Saltzmann) for enhanced elasticity. Last, on a circular knitting machine (Mayer Relanit 0.8, Mayer & Cie), copper knitwear was produced out of 0.10-mm copper wire (Leoni Draht GmbH) using a stockinette stitch construction.

Materials

Pyrrole (Py; Sigma-Aldrich) and EDOT (H.C. Starck) were freshly distilled at reduced pressure and stored in the dark under inert atmosphere at low temperature. Lithium bis(trifluoromethanesulfonyl)imide (LiTFSI, 99:0%; Sigma-Aldrich). Fe(III) tosylate was received from H.C. Stark as a 55 wt % solution in *n*-butanol. Poly(ethylene glycol) dimethacrylate (PEGDM; M_w = 750 g/mol) and poly(ethylene glycol) methyl ether methacrylate (PEGM, M_w = 475 g/mol) were received from Sigma-Aldrich. All solutions for the electrochemical synthesis of PPy were degassed in an ultrasonic bath and saturated with N_2 for 10 min before use.

Two-step chemical-electrochemical combined PEDOT-PPy synthesis

Oxidative VPP of EDOT.

VPP PEDOT on Lyocell-based yarns and textiles was carried out in a single chamber vacuum setup. PEGDM (15 wt %) and PEGM (15 wt %) were dissolved in the 55 wt % $Fe(Tos)_3$ solution in *n*-butanol. The yarn or textile was coated with the oxidant solution by dip coating. The coated yarn or textile was then transferred to the polymerization chamber (heated vacuum chamber from Grupo-Selecta) containing a petri dish with 200 µl of freshly distilled EDOT and maintained at 40°C for 120 min at 1 mmHg pressure. Thereafter, the coated yarn or textile was taken out, thoroughly washed several times with ethanol, and dried at room temperature at a pressure of 1 mmHg for 4 hours.

Electrochemical synthesis of PPy.

Electrochemical synthesis of the PPy on the chemically synthesized PEDOT was carried out in a three-electrode electrochemical cell containing pyrrole (0.1 M) as a monomer and LiTFSI (0.1 M) as a dopant dissolved in propylene carbonate (fig. S2). The chemically PEDOT-coated yarn or textile was used as working electrode, the gold-coated polyethylene (PET) substrate was used as a counter electrode, and a Ag/Ag^+ nonaqueous electrode was used as a reference electrode. PPy synthesis was carried out at a current density of 0.1 mA cm^{-2} at a temperature of −18°C for 20,000 s.

Isometric force and isotonic strain measurements

The individual yarn and textile actuator (length = 20 mm for individual yarns and fabrics) testing was performed using the Lever Arm Dual Mode Servo System (series 300B, Cambridge Technology) that enables forces from 0 to 50 g and displacements length excursion from 0 to 10 mm. Cu tape (double-sided, from 3M no. 1182 acquired from Elfa Distrelec) was attached to both ends as mechanical and electrical contacts. The textile actuators were clamped at the lower end and connected to the lever arm by a stainless steel wire at the upper end (fig. S5). Testing was performed by immersing the conductive yarn or textile in a three-electrode system consisting of a nonaqueous Ag/Ag^+ reference electrode, a gold-coated PET substrate counter electrode, and the yarn or textile sample as the working electrode. A 0.1 M LiTFSI in PC solution was used as the electrolyte. The potential was scanned between 0.5 and −1 V to drive the sample between the oxidized and reduced states. Electromechanical characterizations of the textile actuators were performed in both isometric and isotonic states (*41*). For the isometric force measurement, the lever arm force was initially set higher than what the actuator is capable of generating. An initial preload force (1 g) was then applied to the actuator when the CP was in its reduced state (expanded state). Switching the polymer (that is, PPy) between its reduced and oxidized states by applying 0.5 V caused an increase in the force that can be monitoring by observing the change of voltage. The isometric force generated by the actuator was determined from the difference in maximum force and the preload force. For isotonic strain measurement, similar initial preload (1 g) was applied to the actuator. The actuator contracted during oxidation by applying 0.5 V. The strain was determined by the change in the longitudinal displacement. All reported data were the average of five parallel measurements.

LEGO lever arm

A lever arm was constructed from LEGO technic bricks bought online at www.lego.com, "Pick a Brick." A custom electrochemical cell was constructed from plastic tubing. Cu tape (3M double-sided, no. 1182 from Elfa Distrelec) was attached to both ends as mechanical and electrical contacts. The textile actuators or textuators (~7 cm) were clamped at the lower end and connected to the arm by the holed Cu tape. Approximately 3 cm of the textile was submerged and thereby electromechanically active. A movie was recorded using a Veho VMS-004, 20-400× Magnification USB Digital Microscope Camera with a 2-megapixel Cmos lens (interpolated) and an alloy flexi-stand, and measurement software.

SUPPLEMENTARY MATERIALS

Supplementary material for this article is available at http://advances.sciencemag.org/cgi/content/full/3/1/e1600327/DC1

fig. S1. Illustration of the two-step chemical-electrochemical combined CP synthesis used for the fabrication of the textile actuators.

fig. S2. Schematic illustration of the three-electrode electrochemical cell.

fig. S3. SEM-EDX measurements of the cross section of PEDOT-PPy–coated Lyocell single yarn.

fig. S4. Circumferential strain measurements of the PEDOT-PPy–coated Lyocell single yarn.

fig. S5. Illustration of electrochemical cell configuration used for characterizing the textile actuators.

fig. S6. Stress-strain measurements.
fig. S7. Electromechanical characterizations of the elastane-based textile actuator.
fig. S8. Current transient during the textile actuator life cycle test.
fig. S9. Schematic illustration of the textiles constructions.
fig. S10. Electromechanical characterizations of the copper-based fabric actuator.
table S1. Effect of polyethylene glycol derivatives on the film thickness and electrical conductivity of the VPP PEDOT film.
movie S1. A textuator unit drives a lever arm in a LEGO setup.

REFERENCES AND NOTES

1. Sarcos Corp., http://sarcos.com/ and Ekso Bionics, http://intl.eksobionics.com/.
2. iLimp, hand from Touch Bionics http://touchbionics.com/ and DEKA arm, http://www.dekaresearch.com.
3. D. Rus, M. T. Tolley, Design, fabrication and control of soft robots. *Nature* **521**, 467–475 (2015).
4. D. Trivedi, C. D. Rahn, W. M. Kier, I. D. Walker, Soft robotics: Biological inspiration, state of the art, and future research. *Appl. Bionics Biomech.* **5**, 99–117 (2008).
5. R. F. Shepherd, F. Ilievski, W. Choi, S. A. Morin, A. A. Stokes, A. D. Mazzeo, X. Chen, M. Wang, G. M. Whitesides, Multigait soft robot. *Proc. Natl. Acad. Sci. U.S.A.* **108**, 20400–20403 (2011).
6. J. R. Allen, A. Karchak, R. Snelson, paper presented at the South Western Institute of Radio Engineers Convention, 1962.
7. R. Pelrine, R. Kornbluh, Q. Pei, J. Joseph, High-speed electrically actuated elastomers with strain greater than 100%. *Science* **287**, 836–839 (2000).
8. E. Edqvist, E. Hedlund, B. Lundberg, Quasi-static and dynamic electromechanical response of piezoelectric multilayer cantilever beams. *Sens. Actuators A* **157**, 198–209 (2010).
9. R. H. Baughman, C. Cui, A. A. Zakhidov, Z. Iqbal, J. N. Barisci, G. M. Spinks, G. G. Wallace, A. Mazzoldi, D. De Rossi, A. G. Rinzler, O. Jaschinski, S. Roth, M. Kertesz, Carbon nanotube actuators. *Science* **284**, 1340–1344 (1999).
10. A. Lendlein, S. Kelch, Shape-memory polymers. *Angew. Chem. Int. Ed.* **41**, 2034–2057 (2002).
11. R. Altmüller, R. Schwödiauer, R. Kaltseis, S. Bauer, I. Graz, Large area expansion of a soft dielectric membrane triggered by a liquid gaseous phase change. *Appl. Phys. A* **105**, 1–3 (2011).
12. C. S. Haines, M. D. Lima, N. Li, G. M. Spinks, J. Foroughi, J. D. W. Madden, S. Hyeong Kim, S. Fang, M. Jung de Andrade, F. Göktepe, Ö. Göktepe, S. M. Mirvakili, S. Naficy, X. Lepró, J. Oh, M. E. Kozlov, S. Jeong Kim, X. Xu, B. J. Swedlove, G. G. Wallace, R. H. Baughman, Artificial muscles from fishing line and sewing thread. *Science* **343**, 868–872 (2014).
13. J. Foroughi, G. M. Spinks, G. G. Wallace, J. Oh, M. E. Kozlov, S. Fang, T. Mirfakhrai, J. D. W. Madden, M. K. Shin, S. J. Kim, R. H. Baughman, Torsional carbon nanotube artificial muscles. *Science* **334**, 494–497 (2011).
14. J. A. Lee, R. H. Baughman, S. J. Kim, High performance electrochemical and electrothermal artificial muscles from twist-spun carbon nanotube yarn. *Nano Convergence* **2**, 8 (2015).
15. J. Abel, J. Luntz, D. Brei, A two-dimensional analytical model and experimental validation of garter stitch knitted shape memory alloy actuator architecture. *Smart Mater. Struct.* **21**, 085011 (2012).
16. J. Abel, J. Luntz, D. Brei, Hierarchical architecture of active knits. *Smart Mater. Struct.* **22**, 125001 (2013).
17. J. A. Lee, M. K. Shin, S. H. Kim, H. U. Cho, G. M. Spinks, G. G. Wallace, M. D. Lima, X. Lepró, M. E. Kozlov, R. H. Baughman, S. J. Kim, Ultrafast charge and discharge biscrolled yarn supercapacitors for textiles and microdevices. *Nat. Commun.* **4**, 1970 (2013).
18. L. Liu, Y. Yu, C. Yan, K. Li, Z. Zheng, Wearable energy-dense and power-dense supercapacitor yarns enabled by scalable graphene-metallic textile composite electrodes. *Nat. Commun.* **6**, 7260 (2015).
19. S. Seyedin, J. M. Razal, P. C. Innis, A. Jeiranikhameneh, S. Beirne, G. G. Wallace, Knitted strain sensor textiles of highly conductive all-polymeric fibers. *ACS Appl. Mater. Interfaces* **7**, 21150–21158 (2015).
20. V. Kaushik, J. Lee, J. Hong, S. Lee, S. Lee, J. Seo, C. Mahata, T. Lee, Textile-based electronic components for energy applications: Principles, problems, and perspective. *Nanomaterials* **5**, 1493–1531 (2015).
21. Q. Pei, O. Inganäs, Electrochemical applications of the bending beam method. 1. Mass transport and volume changes in polypyrrole during redox. *J. Phys. Chem.* **96**, 10507–10514 (1992).
22. T. F. Otero, J. Rodriguez, E. Angulo, C. Santamaria, Artificial muscles from bilayer structures. *Synth. Met.* **57**, 3713–3717 (1993).
23. E. W. H. Jager, E. Smela, O. Inganäs, Microfabricating conjugated polymer actuators. *Science* **290**, 1540–1545 (2000).
24. C. Fay, K.-T. Lau, S. Beirne, C. Conaire, K. McGuinness, B. Corcoran, N. E. O'Connor, D. Diamond, S. McGovern, G. Coleman, R. Shepherd, G. Alici, G. Spinks, G. Wallace, Wireless aquatic navigator for detection and analysis (WANDA). *Sens. Actuators B* **150**, 425–435 (2010).
25. E. Smela, O. Inganäs, I. Lundström, Controlled folding of micrometer-size structures. *Science* **268**, 1735–1738 (1995).
26. E. W. H. Jager, O. Inganäs, I. Lundström, Microrobots for micrometer-size objects in aqueous media: Potential tools for single cell manipulation. *Science* **288**, 2335–2338 (2000).
27. J. D. Madden, R. A. Cush, T. S. Kanigan, I. W. Hunter, Fast contracting polypyrrole actuators. *Synth. Met.* **113**, 185–192 (2000).
28. T. Bashir, M. Skrifvars, N.-K. Persson, Production of highly conductive textile viscose yarns by chemical vapor deposition technique: A route to continuous process. *Polym. Adv. Technol.* **22**, 2214–2221 (2011).
29. I. G. Trindade, J. M. da Silva, R. Miguel, M. Pereira, J. Lucas, L. Oliveira, B. Valentim, J. Barreto, M. S. Silva, Synthesis of poly (3, 4-ethylenedioxythiophene) coating on textiles by the vapor phase polymerization method. *Text. Res. J.* **85**, 325–333 (2015).
30. U. Hipler, C. Wiegand, Biofunctional textiles based on cellulose and their approaches for therapy and prevention of atopic eczema, in *Handbook of Medical Textiles*, V. Bartels, Ed. (Elsevier, 2011), pp. 280–294.
31. B. Winther-Jensen, J. Chen, K. West, G. Wallace, Vapor-phase polymerization of pyrrole and thiophene using iron(III) sulfonates as oxidizing agents. *Macromolecules* **37**, 5930–5935 (2004).
32. A. Maziz, C. Plesse, C. Soyer, E. Cattan, F. Vidal, Top-down approach for the direct synthesis, patterning and operation of artificial micromuscles on flexible substrates. *ACS Appl. Mater. Interfaces* **8**, 1559–1564 (2015).
33. D. Melling, S. Wilson, E. W. H. Jager, The effect of film thickness on polypyrrole actuation assessed using novel non-contact strain measurements. *Smart Mater. Struct.* **22**, 104021 (2013).
34. A. Della Santa, D. De Rossi, A. Mazzoldi, Characterization and modelling of a conducting polymer muscle-like linear actuator. *Smart Mater. Struct.* **6**, 23–34 (1997).
35. A. Maziz, A. Khaldi, N.-K. Persson, E. W. Jager, *Soft linear electroactive polymer actuators based on polypyrrole, Proc. SPIE 9430, Electroactive Polymer Actuators and Devices (EAPAD)*, 943016 (2015).
36. J. Torop, A. Aabloo, E. W. Jager, Novel actuators based on polypyrrole/carbide-derived carbon hybrid materials. *Carbon* **80**, 387–395 (2014).
37. X. Wang, E. Smela, Experimental studies of ion transport in PPy(DBS). *J. Phys. Chem. C* **113**, 369–381 (2009).
38. S. Hara, T. Zama, W. Takashima, K. Kaneto, Free-standing polypyrrole actuators with response rate of 10.8% s^{-1}. *Synth. Met.* **149**, 199–201 (2005).
39. G. M. Spinks, L. Liu, G. G. Wallace, D. Zhou, Strain response from polypyrrole actuators under load. *Adv. Funct. Mater.* **12**, 437–440 (2002).
40. S. Hara, T. Zama, W. Takashima, K. Kaneto, Tris(trifluoromethylsulfonyl)methide-doped polypyrrole as a conducting polymer actuator with large electrochemical strain. *Synth. Met.* **156**, 351–355 (2006).
41. G. M. Spinks, T. E. Campbell, G. G. Wallace, Force generation from polypyrrole actuators. *Smart Mater. Struct.* **14**, 406–412 (2005).
42. J. Ding, L. Liu, G. M. Spinks, D. Zhou, G. G. Wallace, J. Gillespie, High performance conducting polymer actuators utilising a tubular geometry and helical wire interconnects. *Synth. Met.* **138**, 391–398 (2003).
43. A. S. Hutchison, T. W. Lewis, S. E. Moulton, G. M. Spinks, G. G. Wallace, Development of polypyrrole-based electromechanical actuators. *Synth. Met.* **113**, 121–127 (2000).
44. S. Hara, T. Zama, W. Takashima, K. Kaneto, Artificial muscles based on polypyrrole actuators with large strain and stress induced electrically. *Polym. J.* **36**, 151–161 (2004).
45. L. Bay, K. West, S. Skaarup, Pentanol as co-surfactant in polypyrrole actuators. *Polymer* **43**, 3527–3532 (2002).
46. J. G. Martinez, T. F. Otero, E. W. H. Jager, Effect of the electrolyte concentration and substrate on conducting polymer actuators. *Langmuir* **30**, 3894–3904 (2014).
47. L. Bay, T. Jacobsen, S. Skaarup, K. West, Mechanism of actuation in conducting polymers: Osmotic expansion. *J. Phys. Chem. B* **105**, 8492–8497 (2001).
48. M. J. M. Jafeen, M. A. Careem, S. Skaarup, Speed and strain of polypyrrole actuators: Dependence on cation hydration number. *Ionics* **16**, 1–6 (2010).
49. S. Hara, T. Zama, W. Takashima, K. Kaneto, Polypyrrole–metal coil composite actuators as artificial muscle fibres. *Synth. Met.* **146**, 47–55 (2004).
50. H. Mao, P. G. Pickup, In situ measurement of the conductivity of polypyrrole and poly [1-methyl-3-(pyrrol-1-ylmethyl) pyridinium]+ as a function of potential by mediated voltammetry. redox conduction or electronic conduction? *J. Am. Chem. Soc.* **112**, 1776–1782 (1990).
51. W. E. Mortan, L. W. Hearle, *Physical Properties of Textile Fibers* (Heinemann, 1975).
52. J. D. Madden, D. Rinderknecht, P. A. Anquetil, I. W. Hunter, Creep and cycle life in polypyrrole actuators. *Sens. Actuators A* **133**, 210–217 (2007).
53. K. Kaneto, T. Shinonome, K. Tominaga, W. Takashima, Electrochemical creeping and actuation of polypyrrole in ionic liquid. *Jpn. J. Appl. Phys.* **50**, 091601 (2011).

54. G. M. Spinks, B. Xi, D. Zhou, V.-T. Truong, G. G. Wallace, Enhanced control and stability of polypyrrole electromechanical actuators. *Synth. Met.* **140**, 273–280 (2004).
55. T. F. Otero, M. Alfaro, V. Martinez, M. A. Perez, J. G. Martinez, Biomimetic structural electrochemistry from conducting polymers: Processes, charges, and energies. Coulovoltammetric results from films on metals revisited. *Adv. Funct. Mater.* **23**, 3929–3940 (2013).
56. D. J. Spencer, *Knitting Technology: A Comprehensive Handbook and Practical Guide* (CRC Press, 2001), vol. 16.
57. H. Hong, M. D. De Araujo, R. Fangueiro, O. Ciobanu, Theoretical analysis of load-extension properties of plain weft knits made from high performance yarns for composite reinforcement. *Text. Res. J.* **72**, 991–996 (2002).
58. A. A. A. Jeddi, A. Zareian, Ideal model for 1× 1 rib fabric taking into account yarn swelling: Guidelines for the use of ultrasonic relaxation. *J. Text. Inst.* **97**, 475–482 (2006).
59. M. Benslimane, P. Gravesen, K. West, S. Skaarup, P. Sommer-Larsen, in *Smart Structures and Materials, EAPAD'99*, Y. Bar-Cohen, Ed. (Proceedings of SPIE, 1999), pp. 87–97.
60. M. Benslimane, P. Gravesen, K. West, S. Skaarup, P. Sommer-Larsen, *1999 Symposium on Smart Structures and Materials* (International Society for Optics and Photonics, 1999), pp. 87–97.
61. A. Maziz, C. Plesse, C. Soyer, C. Chevrot, D. Teyssié, E. Cattan, F. Vidal, Demonstrating kHz frequency actuation for conducting polymer microactuators. *Adv. Funct. Mater.* **24**, 4851–4859 (2014).
62. T. Bashir, M. Ali, N.-K. Persson, S. K. Ramanoorthy, M. Skrifvars, Stretch sensing properties of conductive knitted structures of PEDOT-coated viscose and polyester yarns. *Text. Res. J.* **84**, 323–334 (2014).
63. J. Foroughi, G. M. Spinks, G. G. Wallace, P. G. Whitten, Production of polypyrrole fibres by wet spinning. *Synth. Met.* **158**, 104–107 (2008).
64. W. Lu, A. G. Fadeev, B. Qi, E. Smela, B. R. Mattes, J. Ding, G. M. Spinks, J. Mazurkiewicz, D. Zhou, G. G. Wallace, D. R. MacFarlane, S. A. Forsyth, M. Forsyth, Use of ionic liquids for π-conjugated polymer electrochemical devices. *Science* **297**, 983–987 (2002).
65. A. Punning, K. J. Kim, V. Palmre, F. Vidal, C. Plesse, N. Festin, A. Maziz, K. Asaka, T. Sugino, G. Alici, G. Spinks, G. Wallace, I. Must, I. Põldsalu, V. Vunder, R. Temmer, K. Kruusamäe, J. Torop, F. Kaasik, P. Rinne, U. Johanson, A.-L. Peikolainen, T. Tamm, A. Aabloo, Ionic electroactive polymer artificial muscles in space applications. *Sci. Rep.* **4**, 6913 (2014).

Acknowledgments: We thank A. F. P. Turner for his support, R. Högberg and B. Sklepkovych for their input, L. X. Zhong for help in graphical design, and M. Jager for her help with the LEGO setup. **Funding:** This study was supported by the Carl Trygger Foundation (grant CTS 12:206), the Swedish Research Council (VR-2014-3079), Smart Textiles Initiative (VINNOVA), COST Action MP1003 ESNAM (European Scientific Network for Artificial Muscles), COST-STSM-MP1003-17356, EU FP7 Marie Curie action IEF (625923 POLYACT), Erasmus exchange program of the European Commission, Linköping University, and University of Borås. **Author contributions:** A.M., A.K., N.-K.P., and E.W.H.J. conceived and designed the experiments. N.-K.P. provided the cellulose-based textiles. A.M. carried out most of the experiments. A.C. fabricated and characterized the metal fabric actuator (fig. S10). All authors performed the analysis. A.M., A.K., J.S., N.-K.P., and E.W.H.J. wrote the manuscript, and all authors discussed the results and commented on the manuscript at all stages**. Competing interests:** The authors declare that they have no competing interests. **Data and materials availability:** All data needed to evaluate the conclusions in the paper are present in the paper and/or the Supplementary Materials. Additional data are available from A.M. (ali.maziz@liu.se) upon request.

Submitted 16 February 2016
Accepted 19 December 2016
Published 25 January 2017
10.1126/sciadv.1600327

Citation: A. Maziz, A. Concas, A. Khaldi, J. Stålhand, N.-K. Persson, E. W. H. Jager, Knitting and weaving artificial muscles. *Sci. Adv.* **3**, e1600327 (2017).

Science Advances

Knitting and weaving artificial muscles

Ali Maziz, Alessandro Concas, Alexandre Khaldi, Jonas Stålhand, Nils-Krister Persson and Edwin W. H. Jager

Sci Adv **3** (1), e1600327.
DOI: 10.1126/sciadv.1600327